frontiers

Supplementary Material

Barocaloric Properties of Thermoplastic Elastomers

Naveen Weerasekera[1], Kameswara Pavan Kumar Ajjarapu[1], Kavish Sudan[1], Gamini Sumanasekera[2], Kunal Kate[1], and Bikram Bhatia[1*]

[1]Department of Mechanical Engineering, University of Louisville, KY, USA

[2]Department of Physics and Astronomy, University of Louisville, KY, USA

S1. Materials

Table S1. Materials – supplementary information. Details regarding the materials tested, suppliers/manufacturers, and links for additional information.

Material	Product Name/ Composition	Supplier	URL
SBPI	Styrene 22 wt%	Sigma Aldrich	https://www.sigmaaldrich.com/US/en/product/aldrich/432415
SBPB	Styrene 30 wt%	Sigma Aldrich	https://www.sigmaaldrich.com/US/en/product/aldrich/432490
HYTREL™	Hytrel 6356	DuPont Corporation	https://www.dupont.com/content/dam/dupont/amer/us/en/transportation-industrial/public/documents/en/Hytrel%20Product%20Reference%20Guide.pdf
PIBIFLEX™	PIBIFLEX 2560 NAT	Celanese Corporation	https://www.celanese.com/en/engineered-materials/products/pibiflex-tpc
ESTANE™	ESTANE ALR CL87A	Lubrizole Corporation	http://www.tpucl.com/wp-content/uploads/2021/07/Estane-ALR-CL87A-V.pdf
PELLATHENE™	PELLATHENE 2363 65D	Lubrizole Corporation	https://www.lubrizol.com/Health/Medical/Polymers/Pellethane-TPU
ELVAX™	ELVAX-450, 18% vinyl acetate	Dow Chemicals	https://www.dow.com/en-us/brand/elvax.html
EVCA	Ethylene 32 mol%	Sigma Aldrich	https://www.sigmaaldrich.com/US/en/product/aldrich/414093
PEBAX™	PEBAX 2533	Entec Polymers	https://www.extrememateriels-arkema.com/en/product-families/pebax-elastomer-family/
ZYTEL™	ZYTEL BK031, 33 wt% glass fiber	DuPont Corporation	https://www.dupont.com/products/zytel.html

*Corresponding author
E-mail: bikram.bhatia@louisville.edu

S2. Specific Heat Measurement

The specific heat capacity of all the materials was evaluated using differential scanning calorimetry (DSC). We used the TA Instruments Q-20 calorimeter to perform the measurements at atmospheric pressure. A 12-20 mg sample mass was used in the test pan in addition to an empty reference pan, as per the instrument guidelines. DSC measurements were performed in the 0-400 °C temperature range, with a 10 °C/min heating rate. Figure S1 shows the raw DSC data for all materials tested in this study. The samples were first heated up to their respective melting temperatures and then cooled during the DSC measurement. The data around the extremes of the measurement temperature range – around the material solid-liquid phase change temperature and 0 °C – are omitted for clarity. The temperature dependent specific heat capacity $c_p(T)$ of the material is calculated using the relation,

$$\frac{dQ}{dt} = M.c_p(T).\vartheta, \tag{1}$$

where ϑ is the heating rate in °C/s, M is the sample mass in grams, and $\frac{dQ}{dt}$ is the heat supply rate measured using DSC in Watts.

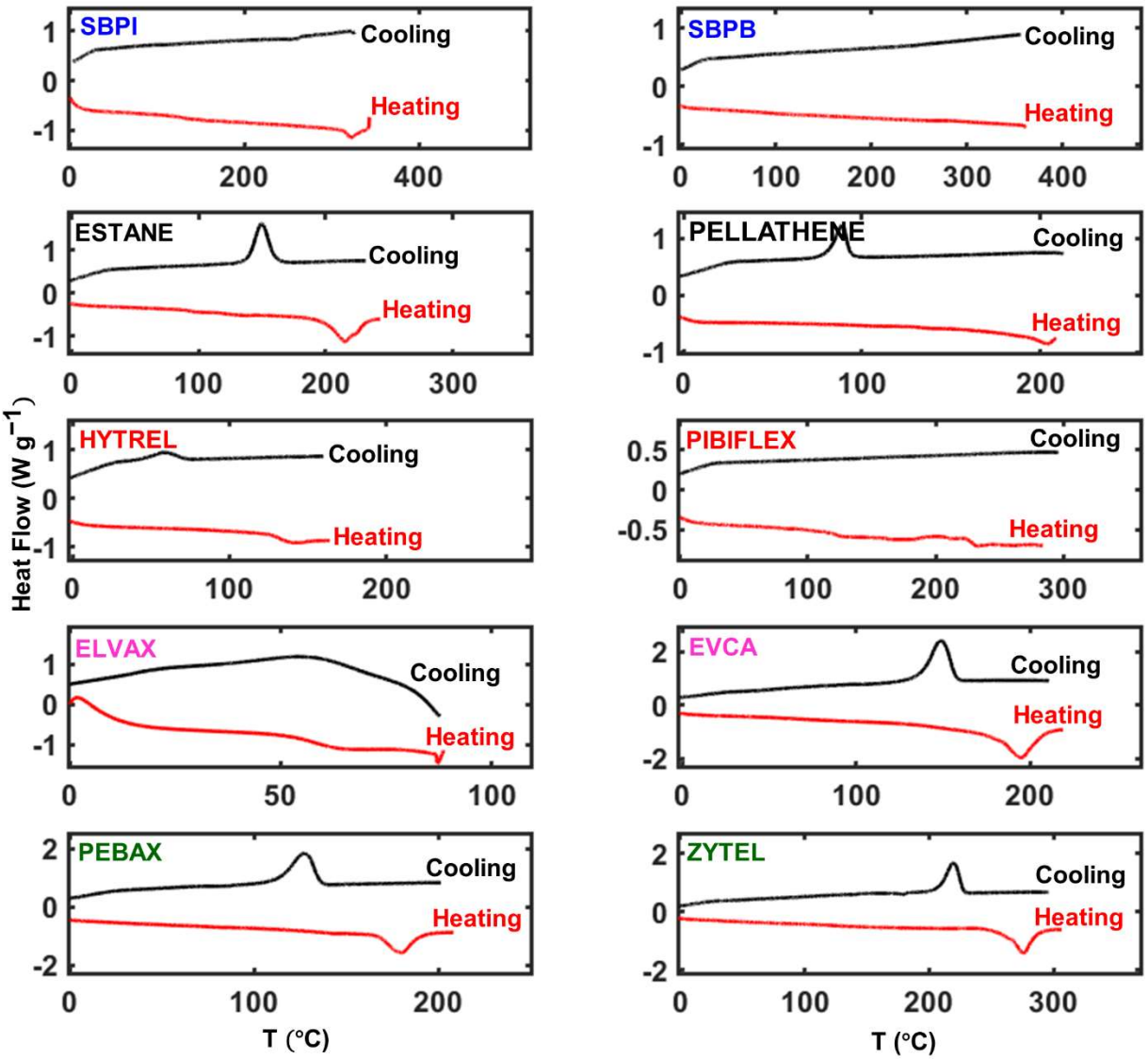

Figure S1. DSC data for all materials. DSC exo- and endotherms of styrenic block copolymers (SBPI and SBPB), thermoplastic polyurethanes (ESTANE and PELLATHENE), thermoplastic copolyesters (HYTREL and PIBIFLEX), thermoplastic polyethylene (ELVAX and EVCA), and thermoplastic polyamides (PEBAX and ZYTEL).

S3. Rheological Measurements

We performed rheological measurements to obtain pvT relationships of all materials in the 35-100 °C temperature span and 100-900 bar (10-90 MPa) pressure range using the Goettfert RG-20 rheometer (Figure S2). A constant sample mass of 34 g was used for all materials as recommended by the instrument manufacturer. The pvT tests (Figure S3) nominally included nine isotherms with 8 °C temperature increment, and nine isobars with 100 bar pressure increment and 0.1 °C/min temperature ramp rates. However, the exact temperature and pressure set points for each sample varied from sample-to-sample and were determined automatically by the instrument. The primary sources of measurement error were the tolerances associated with the rheometer force transducer ($\pm$5%) and J-type thermocouple ($\pm$0.75%). These errors were propagated using standard methods and were used to evaluate errors bars for quantities derived from pvT data – β and NRC (Figures 2 and 4 in the main text).

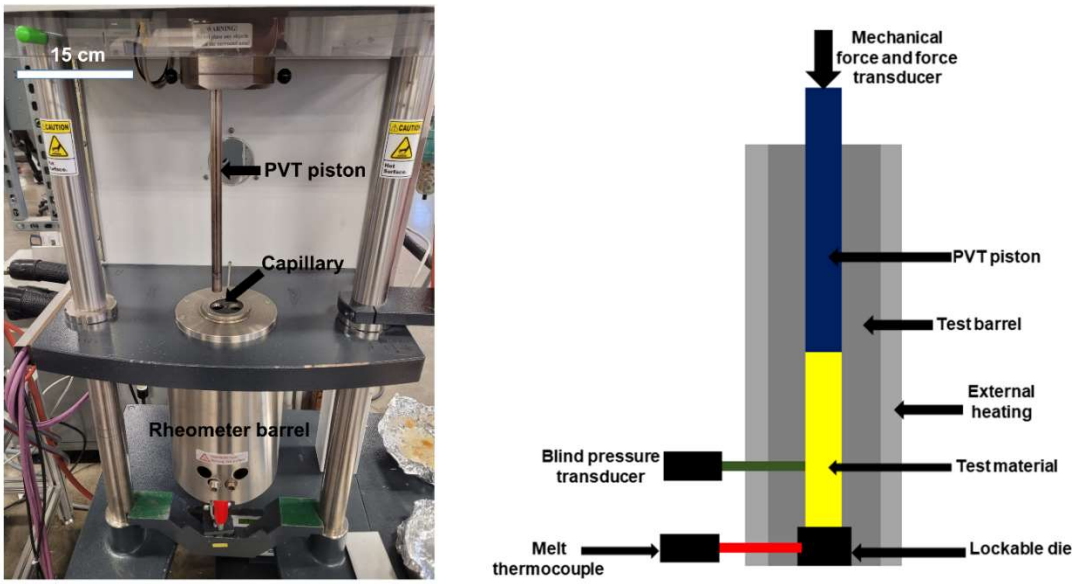

Figure S2. Rheometer setup for pvT measurements. (Left) Photograph of the Goettfert Rheograph RG-20 equipment used for pvT measurements. (Right) Schematic of the rheometer showing the setup for a pvT test.

Each isobar and isotherm is fitted with the two-domain Tait equation of state for solid phase given by (Wang et al. 2019),

$$v(T,p) = v_0(T).\left[1 - C.\ln\left\{1 + \frac{p}{B(T)}\right\}\right] + v_t(T,p) \tag{2}$$

where v_0 is the specific volume at zero applied pressure, v_t is the specific volume decrease due to crystallization, B is the sensitivity to pressure and C is a universal constant 0.0894 given by,

$$v_o(T) = b_{1s} + b_{2s}(T - b_5) \tag{3}$$

$$B(T) = b_{3s}.\exp(-b_{4s}(T - b_5)) \tag{4}$$

$$v_t(T,p) = b_7\exp(b_8(T - b_5) - b_9p) \tag{5}$$

where, b_{1s}, b_{2s}, b_{3s}, b_{4s}, b_7, b_8 and b_9 are model coefficients evaluated by curve fitting.

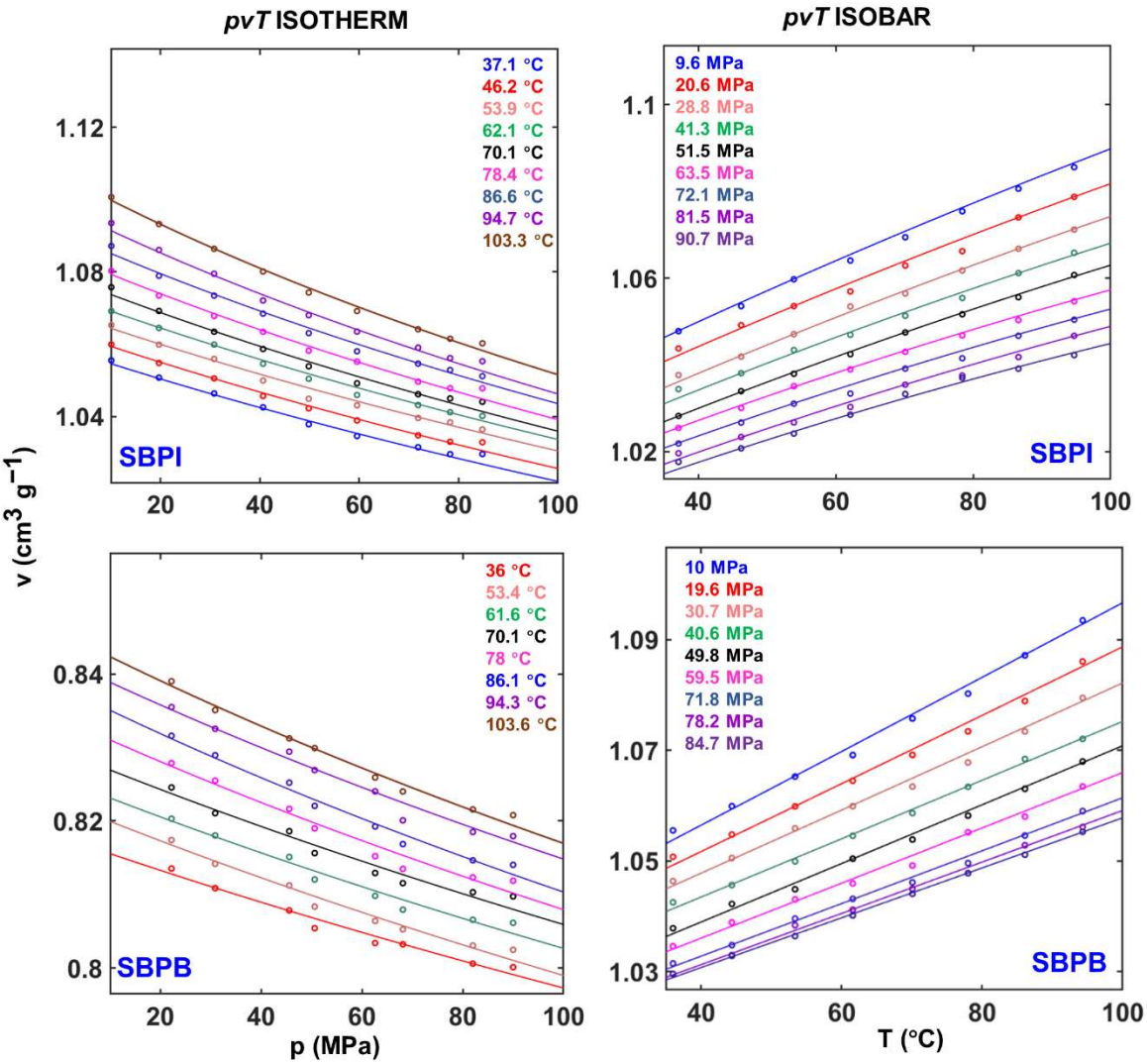

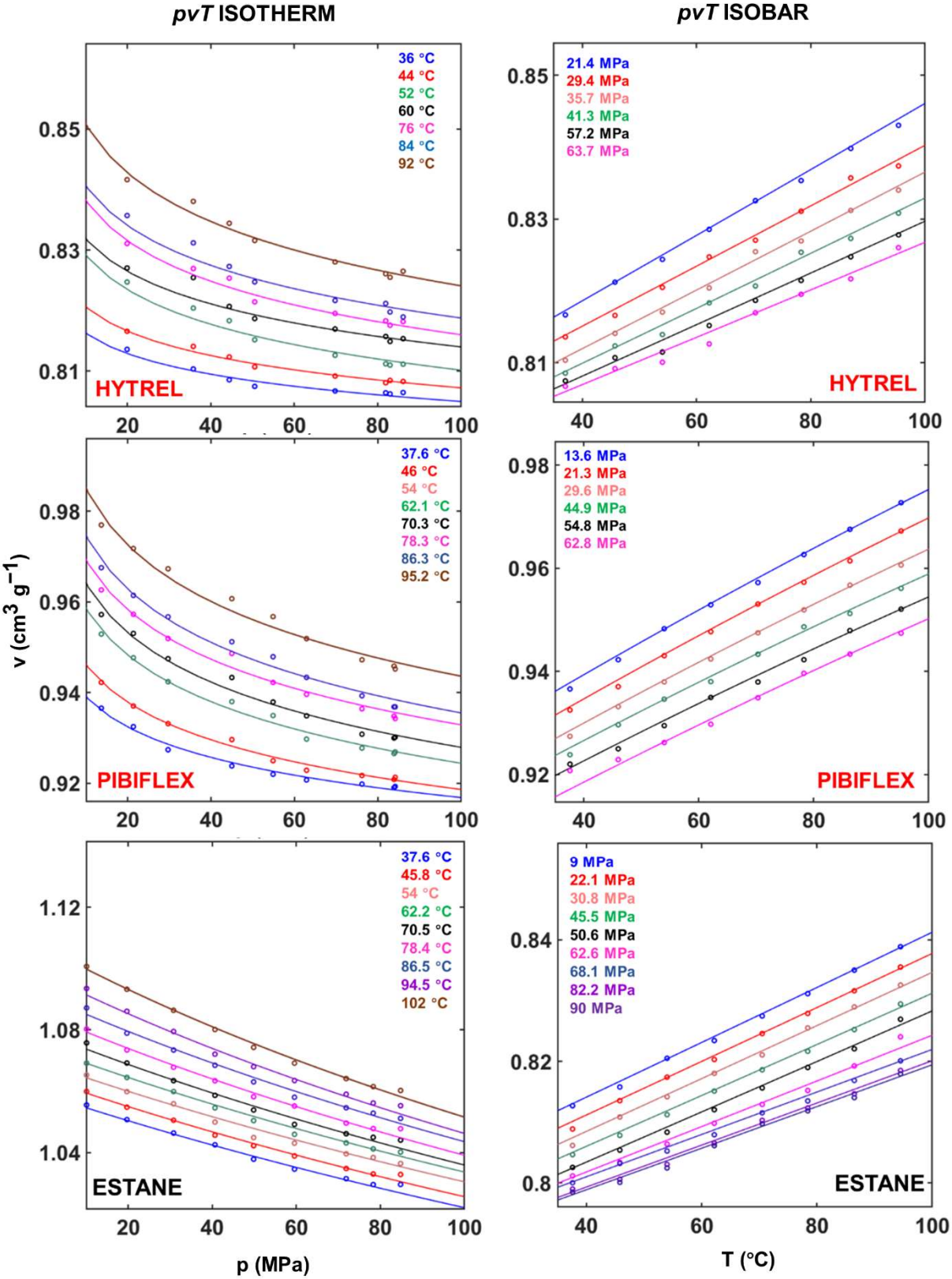
pvT ISOTHERM
pvT ISOBAR
36 °C
44 °C
52 °C
60 °C
76 °C
84 °C
92 °C
HYTREL
21.4 MPa
29.4 MPa
35.7 MPa
41.3 MPa
57.2 MPa
63.7 MPa
HYTREL
37.6 °C
46 °C
54 °C
62.1 °C
70.3 °C
78.3 °C
86.3 °C
95.2 °C
PIBIFLEX
13.6 MPa
21.3 MPa
29.6 MPa
44.9 MPa
54.8 MPa
62.8 MPa
PIBIFLEX
37.6 °C
45.8 °C
54 °C
62.2 °C
70.5 °C
78.4 °C
86.5 °C
94.5 °C
102 °C
ESTANE
9 MPa
22.1 MPa
30.8 MPa
45.5 MPa
50.6 MPa
62.6 MPa
68.1 MPa
82.2 MPa
90 MPa
ESTANE
v (cm3 g−1)
p (MPa)
T (°C)

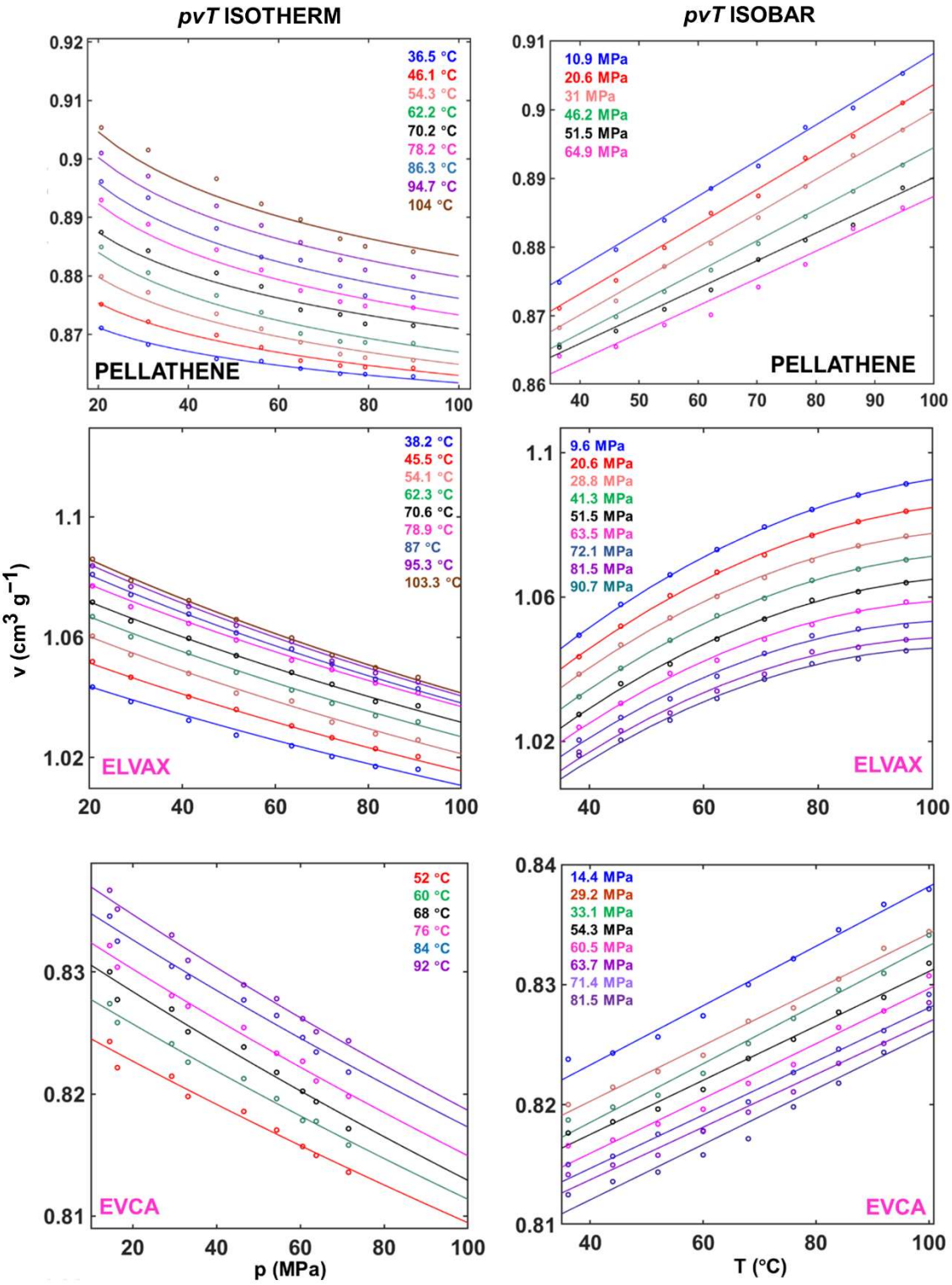
pvT ISOTHERM
pvT ISOBAR
36.5 °C
46.1 °C
54.3 °C
62.2 °C
70.2 °C
78.2 °C
86.3 °C
94.7 °C
104 °C
PELLATHENE
10.9 MPa
20.6 MPa
31 MPa
46.2 MPa
51.5 MPa
64.9 MPa
PELLATHENE
38.2 °C
45.5 °C
54.1 °C
62.3 °C
70.6 °C
78.9 °C
87 °C
95.3 °C
103.3 °C
ELVAX
9.6 MPa
20.6 MPa
28.8 MPa
41.3 MPa
51.5 MPa
63.5 MPa
72.1 MPa
81.5 MPa
90.7 MPa
ELVAX
52 °C
60 °C
68 °C
76 °C
84 °C
92 °C
EVCA
14.4 MPa
29.2 MPa
33.1 MPa
54.3 MPa
60.5 MPa
63.7 MPa
71.4 MPa
81.5 MPa
EVCA
v (cm3 g−1)
p (MPa)
T (°C)

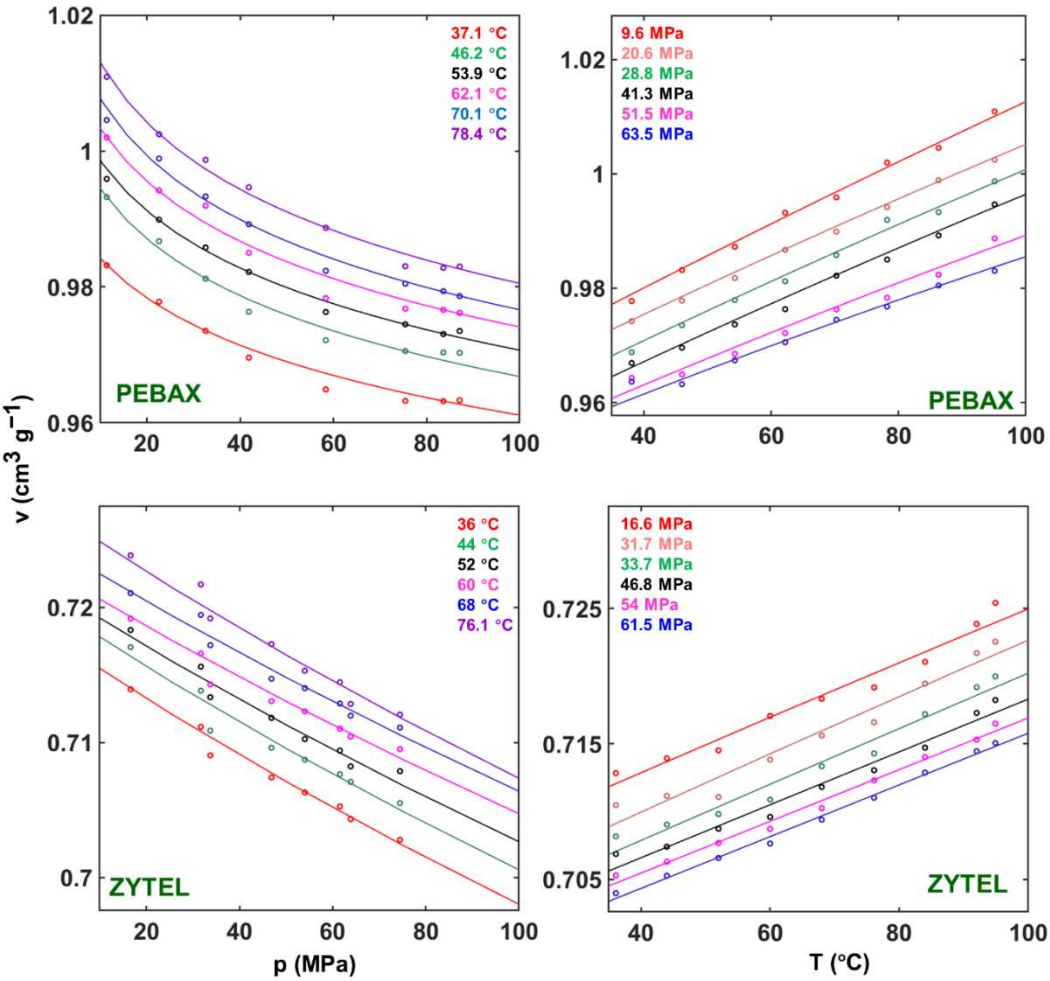

Figure S3. Rheological measurements. pvT isotherms and isobars fitted with the Tait equation of state for all test materials.

S4. Isothermal Volumetric Compressibility Calculation

Isothermal volumetric compressibility (β) of each material was calculated from the pvT isotherms. Gradients $\frac{\partial v}{\partial p}$ are obtained by differentiating the Tait equation of state (Equation 2) with respect to pressure (p). The gradient values are then divided by the initial volume at atmospheric pressure 0.1 MPa (v_0) to obtain volumetric compressibility,

$$\beta = \frac{1}{v_0}\left(\frac{\partial v}{\partial p}\right)_T. \tag{6}$$

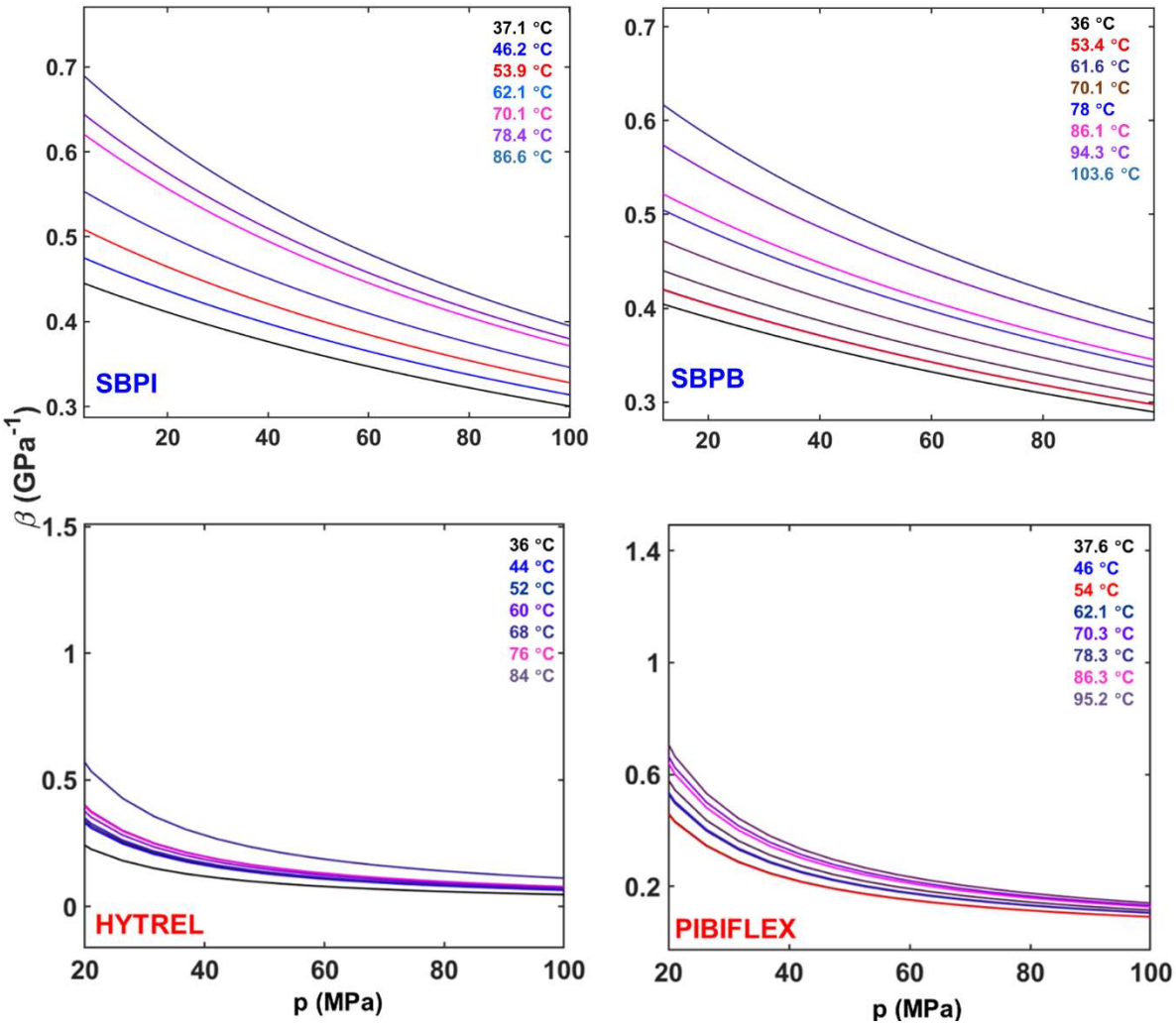

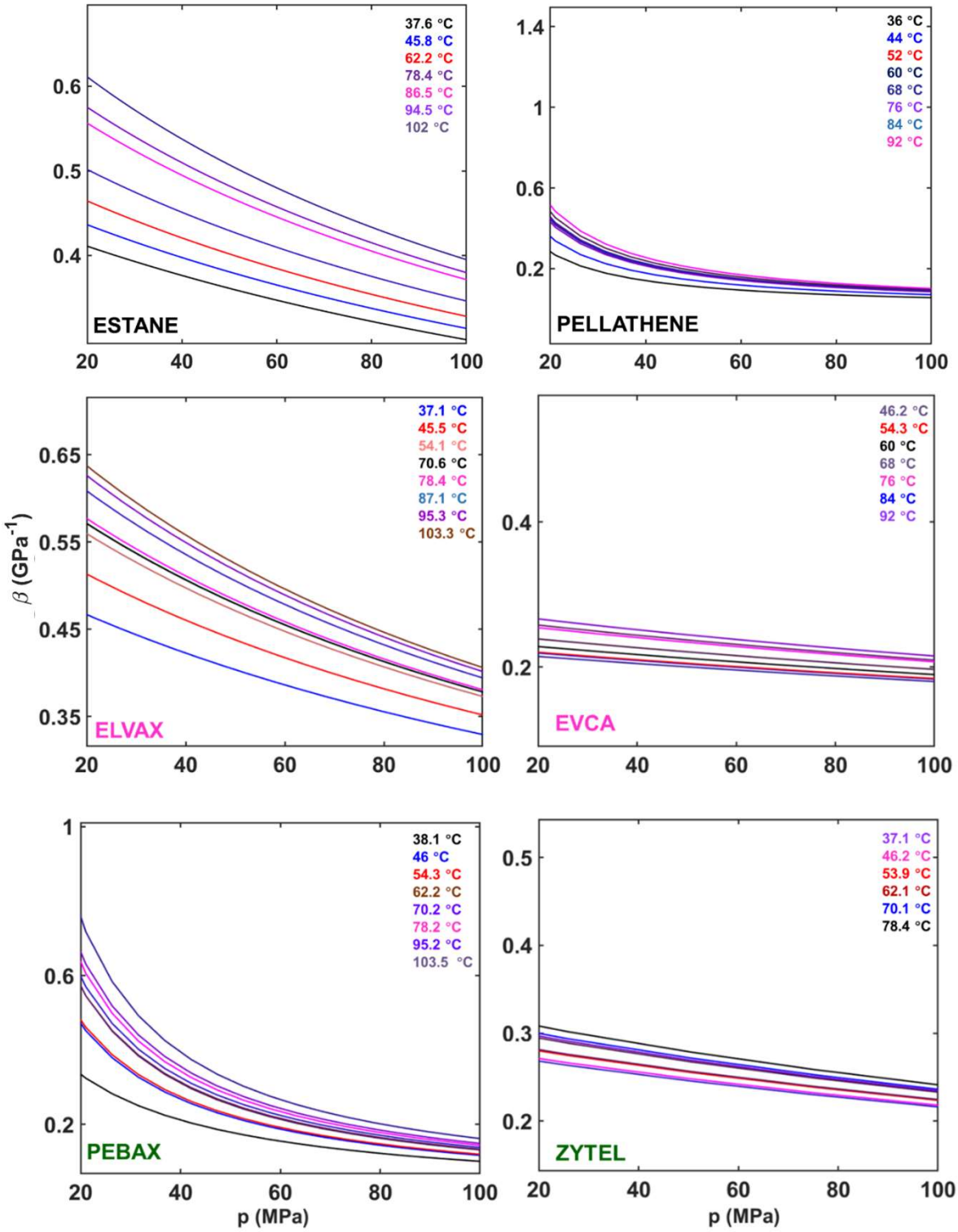

Figure S4. Isothermal compressibility of all materials. Pressure dependence of isothermal volumetric compressibility (β) evaluated using pvT isotherms.

S5. Thermal Conductivity Measurement

The thermal conductivity of all materials was measured using the Goettfert RG-20 rheometer. We used the thermal conductivity probe provided by the manufacturer that operates based on the transient line source method (Hubert Lobo and Claude Cohen 1990). The thermal conductivity probe, which acts as both the heat source and temperature sensor, is dipped in the melted test material as shown in Figure S5. While heat is supplied to the sample, the temperature rise is monitored by the thermocouple (Figure S5). The transient temperature profile is then fitted according to the transient heat conduction equation to obtain the polymer melt thermal conductivity. The error bars in the measured thermal conductivity (Figure 3 in main text) were calculated by accounting for the tolerance of the J-type thermocouple ($\pm$0.75%).

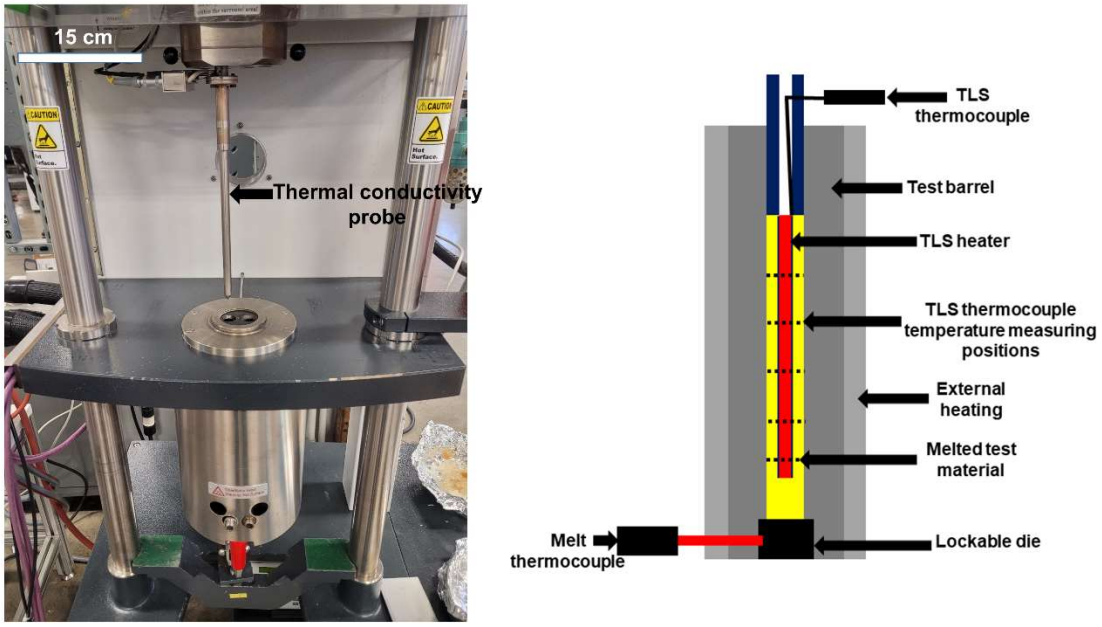

Figure S5. Thermal conductivity measurement setup. (Left) Photograph of the Goettfert RG-20 rheometer used for the thermal conductivity measurement. (Right) Schematic of the setup for the thermal conductivity measurement based on the transient line source method.

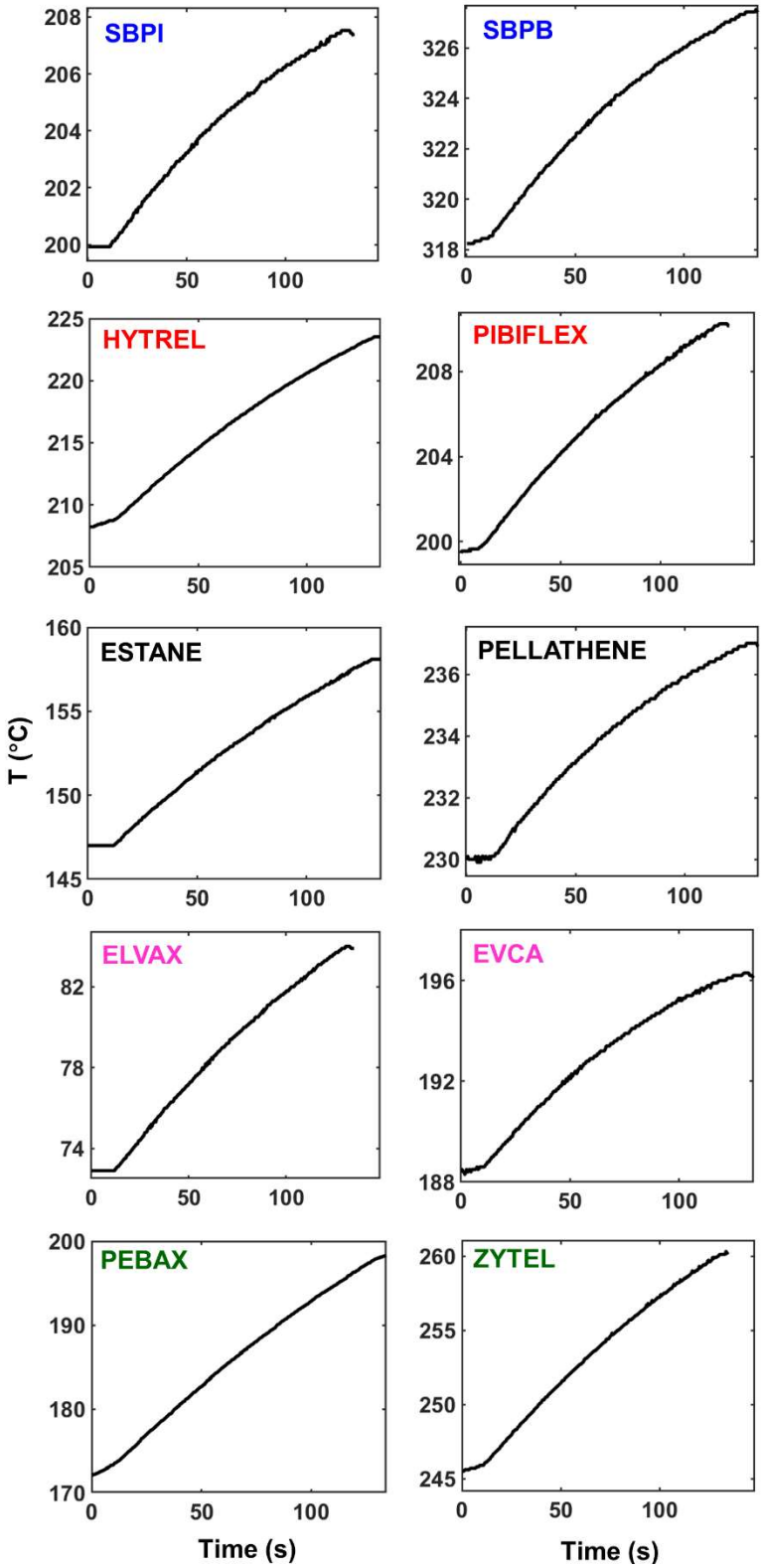

Figure S6. Thermal conductivity measurement data. Transient temperature of all materials as they are heated to evaluate its thermal conductivity.

S6. Normalized Refrigeration Capacity Calculation

The normalized refrigeration capacity (NRC) is calculated for each material (Figure S7) for a chosen temperature ($\Delta T_{h-c} = T_h - T_c$) and pressure range ($\Delta p$) from the pvT isobar data. Initially, we calculated the isobaric volumetric thermal expansion coefficient $\left(\frac{\partial\left(\frac{\Delta v}{v_0}\right)}{\partial T}\right)$ by differentiating the fitted Tait equation of state (Equation 2) with respect to temperature for each isobar. $\left(\frac{\partial\left(\frac{\Delta v}{v_0}\right)}{\partial T}\right)$ is then replotted versus p. The isothermal entropy change ΔS_T is then calculated between pressures p_1 and p_2,

$$\Delta S_T = -v_0 \int_{p_1}^{p_2} \left(\frac{\partial \left(\frac{\Delta v}{v_0}\right)}{\partial T} \right)_p dp. \tag{7}$$

We calculated ΔS_T for different pressure spans $\Delta p = p_2$-p_1 ranging from 20 MPa to 100 MPa, and plotted them with respect to temperature. Finally, NRC is evaluated from the ΔS_T vs T plots (for different Δp values) by integrating over different temperature spans ΔT_{h-c},

$$NRC(\Delta T_{h-c}, \Delta p) = \left| \frac{1}{\Delta p} \int_{T_c}^{T_h} \Delta S_T(T, \Delta p)\, dT \right|. \tag{8}$$

Based on the temperature range of our pvT measurements, we evaluated NRC values for T_c = 35 °C and T_h ranging from 35 °C to 100 °C. Figure S7 shows the NRC vs ΔT_{h-c} plots obtained for all the materials investigated.

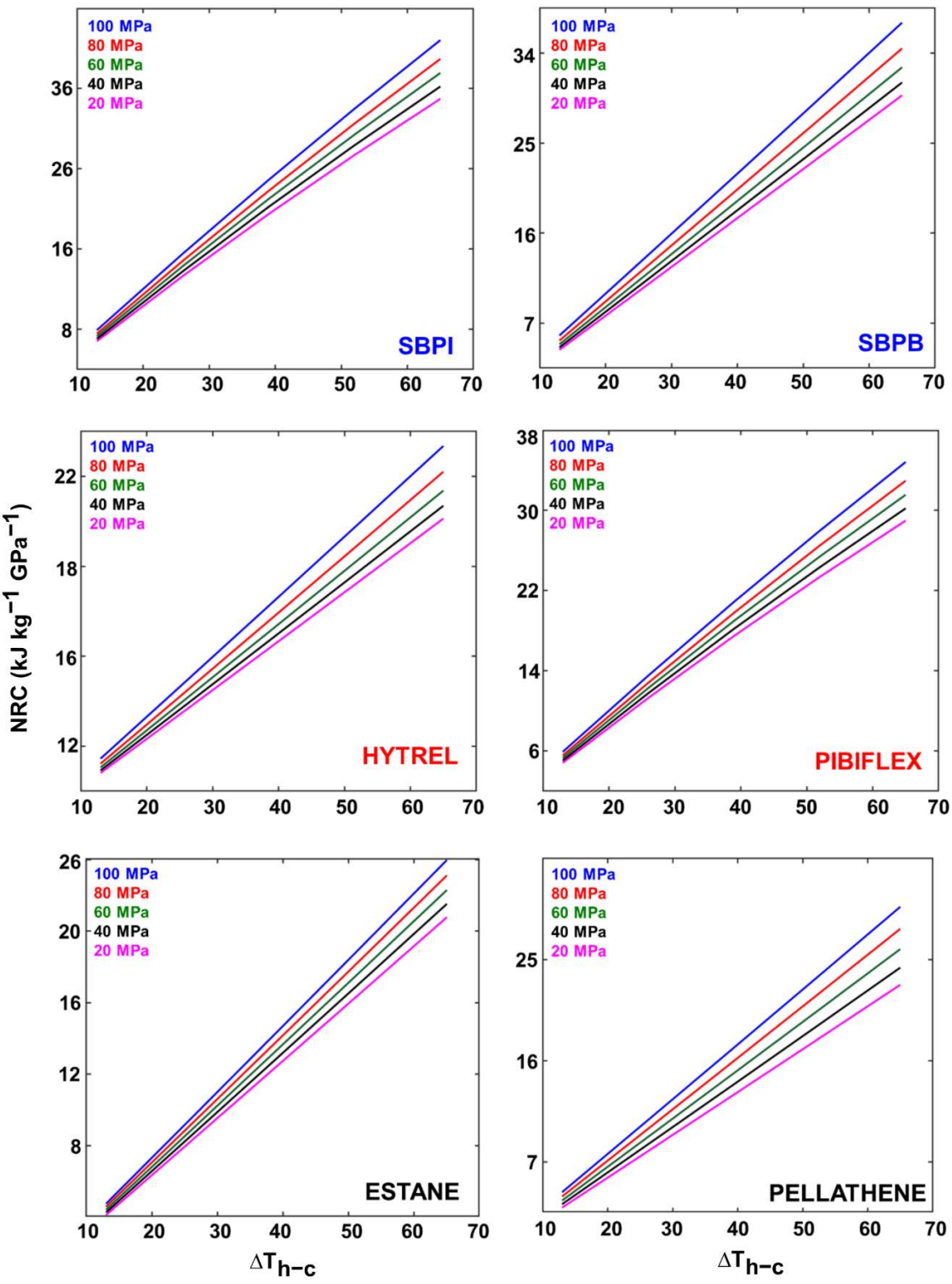
100 MPa
80 MPa
60 MPa
40 MPa
20 MPa
SBPI
SBPB
HYTREL
PIBIFLEX
ESTANE
PELLATHENE
NRC (kJ kg^{-1} GPa^{-1})
ΔT_{h-c}

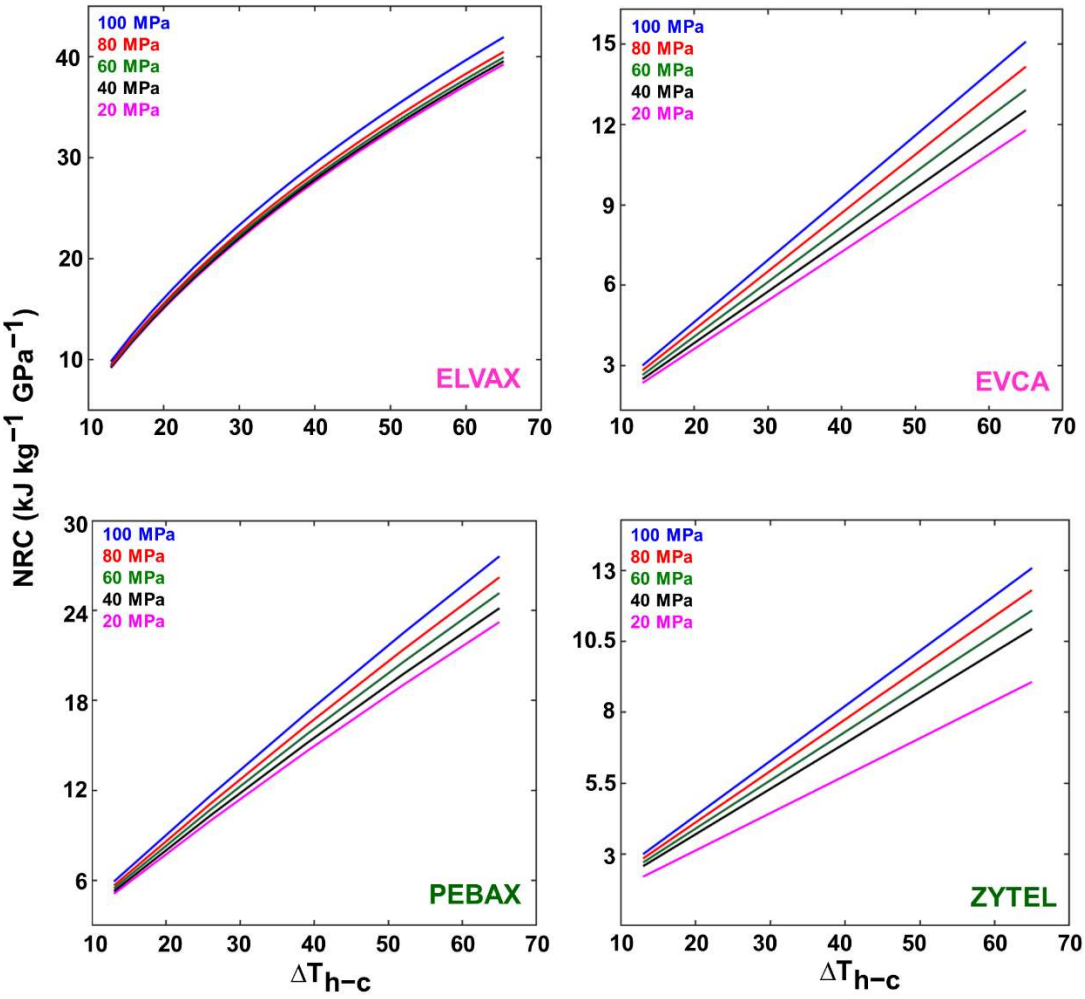

Figure S7. Normalized refrigeration capacity for all materials. NRC values calculated for Δp between 20-100 MPa and ΔT_{h-c} up to 65 °C.

S7. Direct Barocaloric Temperature Change Measurement

Figure S8 shows the quasi-adiabatic BC temperature measurement setup. The setup consists of a sample loading sleeve, piston, top and bottom covers, and a thermocouple surrounded by acrylic resin (to protect the thermocouple from damage when pressure is applied). Samples (mass ~5 g) were loaded into the sleeve in their as-received pellet form. Hydrostatic pressure was applied using an automatic hydraulic press (XRF Scientific AUTO-T40) – force up to 55 kN was applied to the piston with a diameter 10 mm to generate hydrostatic pressures up to 434.1 MPa. Each material was compressed up to a maximum pressure of 276.3-434.1 MPa (corresponding to 35-55 kN force) while measuring its temperature using an embedded K-type thermocouple with a measurement uncertainty of $\pm 0.75\%$. The pressure on the sample was monitored using a load cell built into the press. Each test involved multiple pressure application and release cycles. The temperature of the material was simultaneously measured using an insulated open-ended K-type thermocouple (Omega Engineering) connected to a data acquisition system (Keysight Instruments DAQ-970).

Figure S9 shows the quasi-adiabatic BC temperature change (ΔT_{q-ad}) measured for all materials subjected to five compression-release cycles. (The corresponding errors bars shown in Figure 6 of the main text represent the standard deviation of ΔT_{q-ad} over the five cycles). To ensure consistency across measurements, the duration of each cycle was evaluated based on the thermal time constant (τ) of each material (Bom et al. 2020). The thermal time constant was determined by initially compressing the material to the highest pressure tested (434.1 MPa) and allowing it to cool to ambient temperature over time (t). The resulting temperature $T(t)$ was recorded and fitted to the equation below to calculate τ.

$$T(t) = T_0 + (T_1 - T_0)e^{-(t-t_1)/\tau}, \quad (9)$$

where T_1 is the initial (high) temperature and T_0 is the final (near-ambient) temperature reached after a total time t_1. The material thermal time constant was then used to determine the duration of the pressure application (heating) and pressure release (cooling) steps – approximately 4τ for our measurements.

The measurement setup achieves quasi-adiabatic condition by ensuring the rate of heat loss from the assembly is negligible over the course of the experiments. This was achieved by fabricating

the setup using stainless steel which has relatively low thermal conductivity (~1.5 W m^{-1} K^{-1}). In addition, the measurements were performed at a fast rate – force was applied at a rate of 20 kN/s (thus achieving a maximum force of 55 kN within ~3 s). Thus the time-scale of heat loss from the measurement setup (estimated thermal time constant ~11,650 s) was significantly longer than the measurement time-scale (maximum time for five complete cycles ~3,000 s). Thus, the effect of heat loss from the experimental setup to the surroundings was not significant, and did not affect the direct barocaloric temperature change measurement.

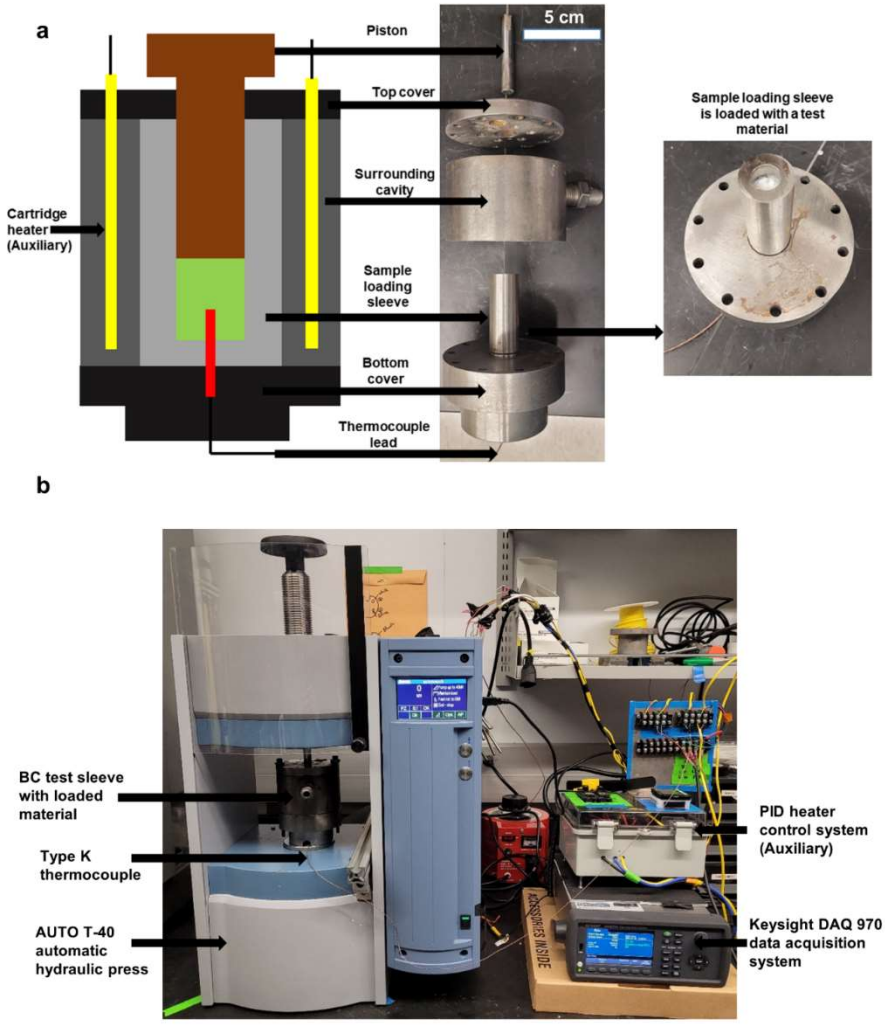

Figure S8. Quasi-adiabatic barocaloric temperature measurement setup. (a) Schematic and photographs showing the key components of the fabricated barocaloric characterization test setup. (b) Photograph of the measurement and data acquisition setup.

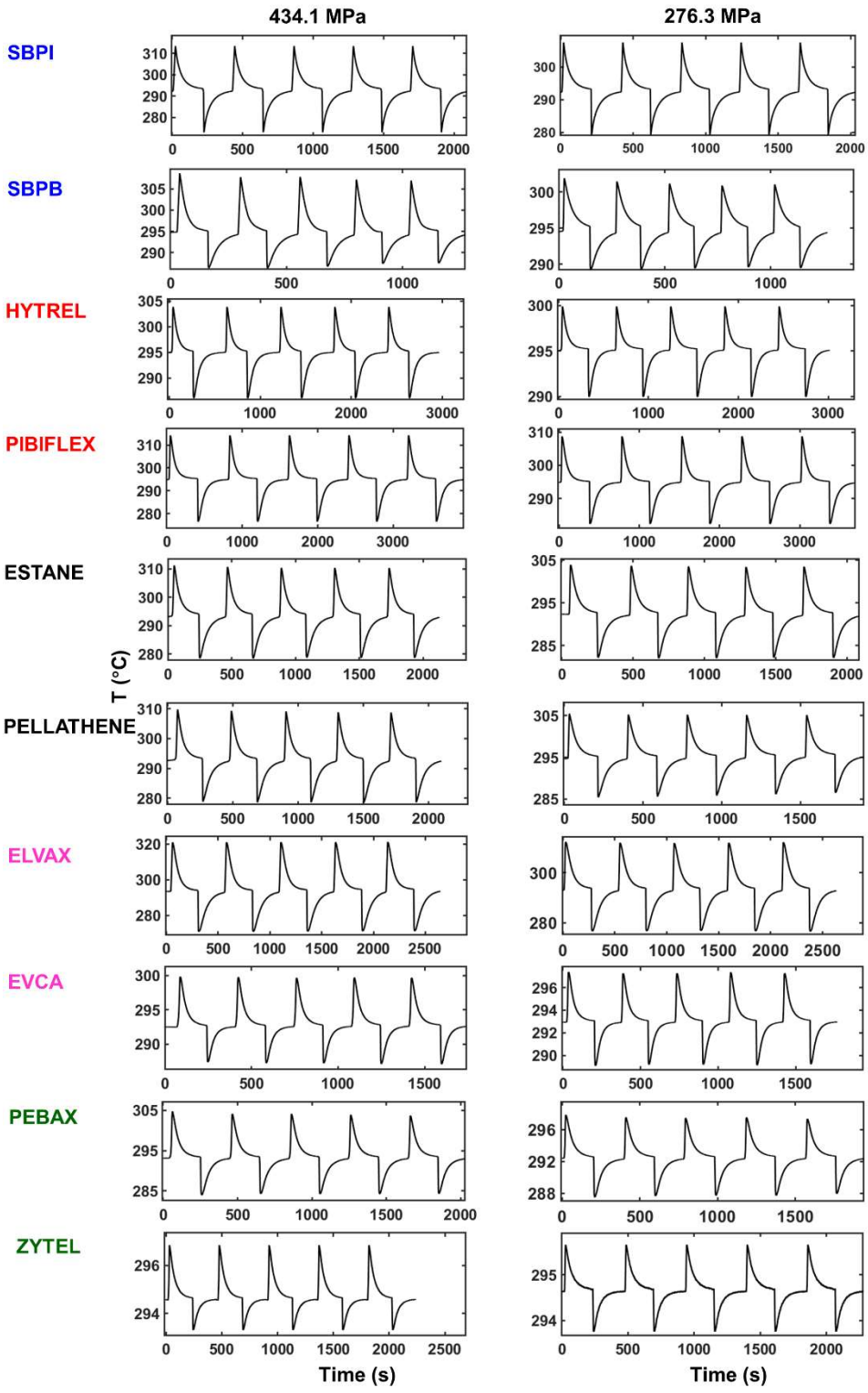

Figure S9. BC temperature change data. Barocaloric material temperature shown for all materials subjected to five compression-release cycles. Data is shown for the highest (434.1 MPa) and lowest pressures (276.3 MPa) tested.

The barocaloric characterization setup used in our measurements applies uniaxial compression which is translated into hydrostatic pressure within the material under investigation. This assumption regarding the hydrostatic pressure is valid in a solid material only if its Poisson's ratio is 0.5. To check this assumption, we calculated the Poisson's ratio of all test materials based on pvT isotherms at 35 ℃ using fundamental solid mechanics relationships for an isotropic material (Lubliner and Papadopoulos 2013),

$$E = 3K(1 - \upsilon) \tag{10}$$

where, E and K are the elastic and bulk modulus of the material, respectively. And υ is the Poisson's ratio. The bulk modulus can be calculated as (Lubliner and Papadopoulos 2013),

$$K = -v_0 \frac{dp}{dv} \tag{11}$$

where, v_0 is the initial specific volume before deformation. The elastic modulus was obtained from the datasheet provided by the manufacturer.

Table S2 shows the calculated Poisson's ratio of all test materials. We note the Poisson's ratio of ZYTEL is 0.34 which suggests the hydrostatic pressure assumption is not strictly valid and, thus, the measured response may not be strictly classified as 'barocaloric'. However, in all other materials the Poisson's ratio is greater than 0.45 indicating the validity of the hydrostatic pressure assumption (Usuda et al. 2019).

Table S2. Calculated Poisson's ratio of test materials

Material	Poisson's Ratio
SBPI	0.500
SBPB	0.500
ESTANE	0.499
PELLATHENE	0.497
HYTREL	0.471
PIBIFLEX	0.477
ELVAX	0.497
EVCA	0.476
PEBAX	0.451
ZYTEL	0.345

S8. Calculation of Materials Coefficient of Performance

We calculated the coefficient of performance (COP) of the materials tested using the method described by Carvalho et al. (Carvalho et al. 2018). The COP is defined as the ratio of heat removed (Q) and input mechanical work (W),

$$\mathrm{COP} = \frac{|Q|}{W} = \frac{T.\Delta S_T}{v_0 \int_{\frac{\Delta v_1}{v_0}}^{\frac{\Delta v_2}{v_0}} p.d\left(\frac{\Delta v}{v_0}\right)} \tag{12}$$

where, T is the working temperature, ΔS_T is the isothermal entropy change resulting from a pressure (p) change corresponding to a normalized specific volume change from $\frac{\Delta v_1}{v_0}$ to $\frac{\Delta v_2}{v_0}$, and v_0 stands for the initial specific volume.

We evaluated the material COP using *pvT* data at a temperature 35 ℃ for a pressure change of 100 MPa (reported in Table 2 in the main text). The pvT isotherm data was used to obtain a relationship between normalized specific volume and pressure for each material. The area under these curves were used to obtain the mechanical work done on the material. The heat removed was evaluated using the isothermal entropy change values calculated earlier – described in Supplementary Materials section 6.

References

Bom, Nicolau Molina, Érik Oda Usuda, Mariana da Silva Gigliotti, Denílson José Marcolino de Aguiar, William Imamura, Lucas Soares Paixão, and Alexandre Magnus Gomes Carvalho. 2020. "Waste Tire Rubber-Based Refrigerants for Solid-State Cooling Devices." *Chinese Journal of Polymer Science* 38 (7): 769–75. https://doi.org/10.1007/s10118-020-2385-y.

Carvalho, A.M.G., W. Imamura, E.O. Usuda, and N.M. Bom. 2018. "Giant Room-Temperature Barocaloric Effects in PDMS Rubber at Low Pressures." *European Polymer Journal* 99 (February): 212–21. https://doi.org/10.1016/j.eurpolymj.2017.12.007.

Hubert Lobo and Claude Cohen. 1990. "Measurement of Thermal Conductivity of Polymer Melts by the Line-Source Method." *Polymer Engineering and Science, Wiley* 30 (2). https://doi.org/10.1002/pen.760300202.

Lubliner, Jacob, and Panayiotis Papadopoulos. 2013. *Introduction to Solid Mechanics: An Integrated Approach*. 1st ed. Springer New York.

Usuda, E. O., W. Imamura, N. M. Bom, L. S. Paixão, and A. M. G. Carvalho. 2019. "Giant Reversible Barocaloric Effects in Nitrile Butadiene Rubber around Room Temperature." *ACS Applied Polymer Materials* 1 (8): 1991–97. https://doi.org/10.1021/acsapm.9b00235.

Wang, Jian, Christian Hopmann, Mauritius Schmitz, Tobias Hohlweck, and Jens Wipperfürth. 2019. "Modeling of PvT Behavior of Semi-Crystalline Polymer Based on the Two-Domain Tait Equation of State for Injection Molding." *Materials & Design* 183 (December): 108149. https://doi.org/10.1016/j.matdes.2019.108149.